

# Cubature Split Covariance Intersection Filter-Based Point Set Registration

Liang Li, *Student Member, IEEE*, Ming Yang<sup>ID</sup>, Chunxiang Wang, and Bing Wang

**Abstract**—Point set registration is a basic but still an open problem in numerous computer vision tasks. In general, there are more than one type of error sources for registration, for example, noise, outliers, and false initialization, may exist simultaneously. These errors could influence the registration independently and dependently. Previous works usually test performance under one of the two types of errors at one time, or they do not perform well under some extreme situations with both of the error sources. This paper presents a robust point set registration algorithm under a filtering framework, which aims to be robust under various types of errors simultaneously. The point set registration problem can be cast into a non-linear state space model. We use a split covariance intersection filter (SCIF) to capture the correlation between the state transition and the observation (moving point set). The two above-mentioned types of errors can be represented as dependent and independent parts in the SCIF. The covariance of the two types of errors will be updated every iteration. Meanwhile, the non-linearity of the observation model is approximated by a cubature transformation. First, the recursive cubature split covariance intersection filter is derived based on the non-linear state space model. Then, we use this algorithm to solve the point set registration problem. This algorithm can approximate non-linearity by a third-order term and consider correlations between the process model and the observation model. Compared with other filtering-based methods, this algorithm is more robust and precise. Tests on both public data sets and experiments validate the precision and robustness of this algorithm to outliers and noise. Comparison experiments show that this algorithm outperforms the state-of-the-art point set registration algorithms in certain respects.

**Index Terms**—Point set registration, cubature split covariance intersection filter, continuous simulated annealing, evolution algorithm.

## I. INTRODUCTION

REGISTRATION of two point sets is a fundamental problem in the field of computer vision and robotics. Corruption of the point set itself and uncertain initial relation between the two point sets make this problem still challenging. Among all the interference factors for point set registration,

Manuscript received May 25, 2017; revised January 29, 2018; accepted March 19, 2018. Date of publication April 6, 2018; date of current version May 16, 2018. This work was supported in part by the National Natural Science Foundation of China under Grant U1764264 and in part by the International Chair on Automated Driving of Ground Vehicle. The associate editor coordinating the review of this manuscript and approving it for publication was Dr. Nilanjan Ray. (*Corresponding author: Ming Yang.*)

The authors are with the Department of Automation, Shanghai Jiao Tong University, Shanghai 200240, China, and also with the Key Laboratory of System Control and Information Processing, Ministry of Education of China, Shanghai 200240, China (e-mail: mingyang@sjtu.edu.cn).

Color versions of one or more of the figures in this paper are available online at <http://ieeexplore.ieee.org>.

Digital Object Identifier 10.1109/TIP.2018.2823427

noise, outliers, bad initialization and missing partial structures are representative. Early works perform well on point sets without interference [1]–[4]. But for more complex registration tasks, these algorithms could only work well to a very limited extent. Classic algorithms such as Iterative Closest Point (ICP) works well in easy situations, for example, missing partial structures in one point set. But it is very likely to converge to a local minimum if the initialization error is beyond some value. Traditional methods such as ICP and Normal Distribution Transform (NDT) [5] require that the two point sets overlap each other for a large part initially. For large misalignment initialization (greater than 90°), high level of noise, outliers, etc., these methods perform poorly for registration.

According to the transform between the two point sets, there are two types of point set registration: rigid and nonrigid. For rigid point set registration, only two types of rigid transform are considered: translation and rotation. Classic applications include Simultaneous Localization And Mapping (SLAM) in robotics [6], feature matching in image processing [7], and structure from motion in computer vision [8]. For nonrigid point set registration, deformation is also included. Classic applications include fingerprint recognition [9], expression recognition [10], and object deformation detection [11]. This paper focuses on the rigid case. Modeling point set registration as a filtering problem has drawn new research interest recently. Li *et al.* [12] use cubature Kalman filtering to solve the point set registration problem. Experimental results in that paper demonstrate substantial improvement over some state-of-the-art algorithms in terms of noise, outliers, misalignment initialization and missing partial structures. However, there is one significant problem that was not investigated in that paper: performance of the algorithm under various error sources simultaneously, *i.e.*, test of existing noise, outliers, misalignment initialization and so forth at the same time. These error sources could degenerate the registration independently and relevantly. Take the noise and outliers for example, they both could influence the correspondence finding. Thus, the correlation of various types of error sources should be considered when they exist simultaneously. In [12], these two types of error sources are not differentiated but included in the fusion framework completely. It can be foreseen that the registration result is inconsistent when these two types of errors exist simultaneously.

In this paper, CSCIF is used to present these two types of errors. In the fusion stage, dependent state and covariance  $\mathbf{X}_d$ ,  $\mathbf{P}_d$ , independent state and covariance  $\mathbf{X}_i$ ,  $\mathbf{P}_i$  are differentiated

to address different error sources. Work present in [12] can be treated as a special case of work presented in this paper. Compared to previous work, the contributions of this paper are threefold:

1. Correlation and independence of various error sources that degenerate registration are considered in this paper. They will be tackled separately and combined in the proposed scheme.
2. We combine the cubature transform and split covariance intersection filter, which will be used to derive a nonlinear solution with the dependent and independent parts of the process and observation model. And we adopt the cubature split covariance intersection filter (CSCIF) for the point set registration problem. This will make the registration more accurate and efficient, in particular when addressing these two types of errors simultaneously; we also investigate this case through tests and experiments.
3. We adopt two heuristic algorithms for covariance and weight optimization, which will improve efficiency of the proposed algorithm.

The remainder of this paper is organized as follows. Section II introduces the related work. The problem formulation is presented in Section III. In Section IV, the cubature transformation and split covariance intersection filter is briefly reviewed, and the CSCIF is derived. Section V describes the point set registration algorithm based on the CSCIF discussed in Section IV. Experiments and comparisons are presented in Section VI. Finally, Section VII concludes this paper.

## II. RELATED WORKS

This section gives an overview on the widely used and state-of-the-art rigid point set registration algorithm. One of the early and widely used methods is ICP [1]. It breaks point set registration into two steps: correspondence establishment and distance optimization. The first step relies on closest point assumption to define correspondences between point sets; *i.e.*, the corresponding point is the closest point in another point set under Euclidean distance. The second step defines distance based on the sum distance of the correspondence and then optimizes the distance using a quaternion-based method. In order to address noise, EM-ICP [13] is proposed. For robustness to the local minimum, GO-ICP [14] is proposed. Biber and Straßer [5] rasterize the point cloud, and every grid is represented by a Gaussian distribution with centroid and covariance. Instead of defining point correspondence, it defines the grid correspondence for robustness to noise and outliers.

Recently, some works model the point set as a Gaussian Mixture Model (GMM) and then compute the similarity of the two point sets. CPD [2] model one point set as GMM and compute the probability that the other point set is represented by this modeled GMM. Unlike ICP or its variant, CPD does not establish correspondence but assigns soft correspondence for all points. Experimental results therein demonstrate substantial improvement of robustness to noise, outliers, and misalignment initialization compared with ICP. GMM-L2 [3] models both point sets as GMMs and computes similarity of the two GMMs. The similarity of the two GMMs is

measured by the L2 distance between these two Gaussian mixtures. The optimization relied on a numerical optimization method (e.g., a quasi-Newton algorithm). It is verified that for rigid registration, GMM-L2 equals a kernel correlation-based algorithm [15]. Experimental results show that it has a wider convergence range than CPD.

More recently, point set registration modeled as a filtering problem achieves good results. In [4], point set registration is modeled as a nonlinear filtering problem and solved by Unscented Kalman Filter (UKF). Experimental results therein show it outperforms ICP in many aspects because of the filtering framework. But point set is not treated as an entire part; points are added one by one as the iterations proceed. Sandhu *et al.* [16] use Particle Filter (PF) to solve the filtering problem. In the measurement update, it relies on ICP to update particles' weights. Thus, it can be seen as a generalized version ICP. Li *et al.* [12] follow the idea to model point set registration as a nonlinear filtering problem. They use Cubature Kalman Filter (CKF) to solve the filtering problem. The Cubature rule is used therein, which can approximate nonlinearity in three orders. Experimental results demonstrate CKF based algorithm outperforms some state-of-the-art registration methods, and the robustness to error sources such as noise, outliers, misalignment initialization and missing partial structures has been improved substantially. But there also exists one problem: It did not take into consideration the correlation of error sources on the filtering model. For example, what if noise, outliers, misalignment initialization, *etc.* exist simultaneously. Some of them may affect time updates more, and others may affect measurement updates more. Some of them are constant during registration, and some of them may change. Thus, the error sources could be treated as a dependent part and an independent part and addressed accordingly.

This paper presents a filtering-framework-based point set registration algorithm. Herein, the cubature split covariance intersection filter is proposed to address the above-mentioned dependent error sources and independent error sources. In CSCIF-based point set registration, the independent error source is modeled as the independent covariance, and the dependent error source is modeled as the dependent covariance, which changes as the iteration proceeds. Besides, the covariance and weights are both optimized by heuristic algorithms, which makes this algorithm robust to falling into the local minimum. Finally, both tests on public 2D and 3D datasets and experiments validate the precision and robustness of this algorithm to outliers, noise and partial structures. Comparison experiments show that this algorithm outperforms state-of-the-art point set registration algorithms in some aspects. More than one error source is also added to test the performance of various algorithms. In the following sections, we will give more details about our method.

## III. PROBLEM FORMULATION

The method for point set registration modeled by the filtering framework is depicted in detail in [12]. In this section, we introduce it briefly for better understanding and to be

self-contained for this paper. Given two point sets  $\mathbf{U} = \{u_1, u_2, \dots, u_m\}$  and  $\mathbf{Z} = \{z_1, z_2, \dots, z_n\}$ , where  $u_i, i = 1, \dots, m$  and  $z_j, j = 1, \dots, N$  are all  $d$ -dimensional points, the goal of registration is to find the transform that best aligns the two point sets. For rigid registration, the transform includes rotation and translation. Thus, the registration result is a rotation matrix  $\mathbf{R}$  and a translation vector  $\mathbf{t}$ . Applying the transform to the moving point set  $\tilde{\mathbf{U}} = \mathbf{RU} + \mathbf{t}$ , difference between  $\tilde{\mathbf{U}}$  and  $\mathbf{Z}$  should be minimized. So, the state vector for rigid registration is a 6-dimensional vector  $\mathbf{x} = [\theta_x, \theta_y, \theta_z, t_x, t_y, t_z]$  with three rotational parameters  $\mathbf{x}_\theta = [\theta_x, \theta_y, \theta_z]$  and three translational parameters  $\mathbf{x}_t = [t_x, t_y, t_z]$ . Then, the point set registration is modeled using the following filtering framework:

$$\mathbf{x}_k = \mathbf{x}_{k-1} + \mathbf{e}_{k-1} \quad (1)$$

$$\mathbf{Z}_k = \mathbf{R}_\theta \mathbf{U}_k + \mathbf{x}_t + \mathbf{v}_k \quad (2)$$

Equation (1) is the state transition model with white Gaussian noise  $\mathbf{e}_{k-1} \sim \mathcal{N}(\mathbf{x}_{k-1}; 0, \mathbf{Q}_{k-1})$ . Since we do not have prior knowledge about the transform between the two point sets, the current state could not transit according to the previous state using a theory-formulated model. Herein, we use a stochastic model to proceed the state in a probabilistic space, and the dynamic is driven by the noise  $\mathbf{e}_{k-1}$ . The size of the transition is determined by the noise covariance  $\mathbf{Q}_{k-1}$  probabilistically; thus, it is a significant value that needs to be set carefully. Setting it too large may result in the algorithm having low efficiency. If set too small, the algorithm may not be able to converge to the optimized value. In this paper, the covariance is adjusted dynamically using a heuristic algorithm, which will be given in detail in the next section. Equation (2) is the observation model with white Gaussian noise  $\mathbf{v}_k \sim \mathcal{N}(\mathbf{x}_k; 0, \mathbf{R}_k)$ .  $\mathbf{U}_k = \mathbf{U}$  is the model point set and is fixed during registration.  $\mathbf{Z}_k$  is the corresponding point set permutation from  $\mathbf{Z}$ .  $\mathbf{R}_\theta$  is a rotation matrix obtained from the rotation parameters of the state  $\mathbf{x}_\theta$ , and  $\mathbf{R}_\theta = \mathbf{R}_{\theta_x} \times \mathbf{R}_{\theta_y} \times \mathbf{R}_{\theta_z}$ , where  $\mathbf{R}_{\theta_x}$  is a rotation matrix along the x-axis with angle  $\theta_x$ , and so forth. If the correspondence between two point sets are fully correct and there is no noise, outliers or any other error source in the two point sets, it would be  $\mathbf{Y}_k = \mathbf{R}_\theta \mathbf{U}_k + \mathbf{x}_t$ . But because of various error sources mentioned above, this strict equation is relaxed by the Gaussian noise  $\mathbf{v}_k$ .

The state space model presented in equation (1) and equation (2) is highly nonlinear because of rotation matrix  $\mathbf{R}_\theta$ . So, a linearity strategy or a numerical calculation method should be adopted to solve the filtering problem. In this paper, we use the cubature rule to deal with nonlinearity. Combined with the split covariance intersection filter to deal with dependent and independent error sources depicted above, we derive the cubature split covariance intersection filter, which will be discussed in the following section.

#### IV. MATHEMATICAL PRELIMINARIES

The previous section models point set registration as a non-linear filtering problem. To deal with nonlinearity, we use the cubature rule. There are other alternatives such as unscented transform [17] and Taylor expansion [18], but they are not as

precise as the cubature transformation. The Taylor expansion could only approximate nonlinearity in the first order, and the unscented transform could approximate nonlinearity in the second order, while the cubature transformation could approximate nonlinearity of more than or equal to third order. A split covariance intersection filter is introduced to deal with the two types of error sources mentioned above. So, in this section, some mathematical preliminaries will be given for better understanding of the proposed point set registration algorithm. In the rest of this section, the CSCIF will be described in detail. To ensure a thorough understanding of the motivation of the CSCIF and the reason why it can effectively solve point set registration problems, a brief overview of the cubature transformation and the split covariance intersection filter are first given here. Then, the CSCIF will be derived based on them.

##### A. Cubature Rule

The cubature rule was first proposed by Stroud [19]. It is a numerical integration method for multi-dimensional integrals. In [20], the cubature rule was utilized to approximate the intractable multi-dimensional integrals in the Bayesian filter, which yielded the cubature Kalman filter. In addition, a spherical-radial rule was proposed. Given an integral whose integrand is non-linear with a weighted or probabilistic function  $\omega(x)$ , based on a Monte Carlo idea, the integral can be approximated by

$$\mathbf{I}(\mathbf{f}) = \int_{\mathcal{D}} \mathbf{f}(\mathbf{x}) \omega(\mathbf{x}) d\mathbf{x} \approx \sum_{i=1}^m \omega_i \mathbf{f}(\mathbf{x}_i) \quad (3)$$

In equation (3),  $\mathbf{f}(\mathbf{x})$  is a non-linear function of  $\mathbf{x}$ , and  $\mathbf{x}$  is the n-dimensional state vector  $\mathbf{x} = [x_1, x_2, \dots, x_n]$ . When  $m \rightarrow \infty$ , the numerical approximation is the same as the integral.

The integrand of the filtering problem with Gaussian noise can be decomposed into the *non-linear function*  $\times$  *Gaussian density* form, as shown in equation (4). Applying a spherical-radial transformation, the integral is shown in equation (5).

$$\mathbf{I}(\mathbf{f}) = \int_{\mathcal{D}} \mathbf{f}(\mathbf{x}) \exp(-\mathbf{x}^T \mathbf{x}) d\mathbf{x} \quad (4)$$

$$\mathbf{I}(\mathbf{f}) = \int_0^\infty \int_{U_n} \mathbf{f}(r\mathbf{s}) r^{n-1} \exp(-r^2) d\sigma(\mathbf{s}) dr \quad (5)$$

In equation (5),  $\mathbf{x} = r\mathbf{s}$ , where  $r = \sqrt{\mathbf{x}^T \mathbf{x}}$  is the length of  $\mathbf{x}$  and  $\mathbf{s}^T \mathbf{s} = 1$  is the unit vector, which denotes the direction of  $\mathbf{x}$ . Thus, equation (5) can be decomposed into two parts: the radial integral and the spherical integral. Applying the Monte Carlo idea in equation (3), the radial integral and the spherical integral can be approximated in equation (6) and equation (7), respectively.

$$\int_0^\infty \mathbf{Y}(r) r^{n-1} \exp(-r^2) dr \approx \sum_{i=1}^{m_r} \omega_{r,i} \mathbf{f}(r_i) \quad (6)$$

$$\mathbf{Y}(r) = \int_{U_n} \mathbf{f}(r\mathbf{s}) d\sigma(\mathbf{s}) \approx \sum_{i=1}^{m_s} \omega_{s,i} \mathbf{f}(r\mathbf{s}_i) \quad (7)$$

Combining equation (6) and equation (7) yields equation (8).

$$\mathbf{I}(\mathbf{f}) \approx \sum_{i=0}^{m_s} \sum_{j=0}^{m_r} \omega_{r,i} \omega_{s,j} \mathbf{f}(r_j \mathbf{s}_i) \quad (8)$$

The spherical cubature rule and the radial rule give us a guide for the choice of the sampling points  $r_j$  and  $\mathbf{s}_i$ . Finally, the third-degree cubature rule is shown in equation (9).

$$\mathbf{I}(\mathbf{f}) \approx \sum_{i=0}^n \omega_i [\mathbf{f}(\xi_i) + \mathbf{f}(-\xi_i)] \quad (9)$$

Where  $\omega_i = \frac{1}{2n}$  and  $\xi_i = \sqrt{n} \mathbf{e}_i$ . In addition,  $\mathbf{e}_i$  is a unit vector, with the  $i^{th}$  element being 1.

### B. Split Covariance Intersection Filter

The covariance intersection filter theory was first proposed in [21] to guarantee its fusion consistency irrespective of the fact that the cross-correlations in the errors between different source data are unknown. However, it assumes that the random variables are fully correlated while ignoring the possible independent information about them. Thus, in [22], SCIF is introduced to consider both the dependent and independent parts of the source data. A detailed introduction to the SCIF can be found in [23]; here, we only provide a brief overview of it. Given two sources of data  $\{\mathbf{X}_i, \mathbf{P}_i\}$ ,  $i = 1, 2$ , where  $\mathbf{X}_i$  and  $\mathbf{P}_i$  are the estimate and covariance, respectively, assume that we obtain the fused estimate  $\{\mathbf{X}, \mathbf{P}\}$  with filtering methods. With a Kalman filter, the result is as follows:

$$\mathbf{P}^{-1} = \mathbf{P}_1^{-1} + \mathbf{P}_2^{-1} \quad (10)$$

$$\mathbf{X} = \mathbf{P}(\mathbf{P}_1^{-1}\mathbf{X}_1 + \mathbf{P}_2^{-1}\mathbf{X}_2) \quad (11)$$

The SCIF decomposes the covariance into two parts: dependent and independent parts. Therefore, the two data sources in this case are  $\{\mathbf{X}_i, \mathbf{P}_{i,d} + \mathbf{P}_{i,i}\}$ . In addition, the fusion result is

$$\mathbf{P}^{-1} = \mathbf{P}_{1*}^{-1} + \mathbf{P}_{2*}^{-1} \quad (12)$$

$$\mathbf{X} = \mathbf{P}(\mathbf{P}_{1*}^{-1}\mathbf{X}_1 + \mathbf{P}_{2*}^{-1}\mathbf{X}_2) \quad (13)$$

where

$$\mathbf{P}_{1*} = \mathbf{P}_{1,i} + \frac{1}{\omega} \mathbf{P}_{1,d} \quad (14)$$

$$\mathbf{P}_{2*} = \mathbf{P}_{2,i} + \frac{1}{1-\omega} \mathbf{P}_{2,d} \quad (15)$$

and  $\omega \in [0, 1]$ . As depicted above, the covariance  $\mathbf{P}$  can be decomposed into dependent and independent parts:  $\mathbf{P} = \mathbf{P}_i + \mathbf{P}_d$ .

$$\mathbf{P}_i = \mathbf{P}\mathbf{P}_{1*}^{-1}\mathbf{P}_{1,i}\mathbf{P}_{1*}^{-1}\mathbf{P} + \mathbf{P}\mathbf{P}_{2*}^{-1}\mathbf{P}_{2,i}\mathbf{P}_{2*}^{-1}\mathbf{P} \quad (16)$$

$$\mathbf{P}_d = \mathbf{P}\mathbf{P}_{1*}^{-1}\mathbf{P}_{1,d}\mathbf{P}_{1*}^{-1}\mathbf{P} + \mathbf{P}\mathbf{P}_{2*}^{-1}\mathbf{P}_{2,d}\mathbf{P}_{2*}^{-1}\mathbf{P} \quad (17)$$

### C. Cubature Split Covariance Intersection Filter

The recursive split covariance intersection filter in the non-linear case can be derived based on the cubature rule, SCIF and state space model. As depicted before, in the point set registration algorithm, the process model is linear, while the observation model is non-linear, which can also be observed

in the next section. Assume that the non-linear state space model of the point set registration problem is as shown in equation (18) and equation (19).

$$\mathbf{x}_t = \mathbf{F}_{t-1} \mathbf{x}_{t-1} + \mathbf{B}_{t-1} \mathbf{u}_{t-1} + \mathbf{v}_{t-1} \quad (18)$$

$$\mathbf{y}_t = \mathbf{g}(\mathbf{x}_t, \mathbf{u}_t) + \mathbf{e}_t \quad (19)$$

Where  $\mathbf{x}_t$  is the state vector at time  $t$ ,  $\mathbf{y}_t$  is the observation at time  $t$ , and  $\mathbf{u}_t$  is the control input at time  $t$ . In addition,  $\mathbf{v}_{t-1} \sim \mathcal{N}(0, \mathbf{Q}_{t-1})$ ,  $\mathbf{e}_t \sim \mathcal{N}(0, \mathbf{R}_t)$  are noise.  $\mathbf{A}_{t-1}$  and  $\mathbf{B}_{t-1}$  are the predictive and control matrices, respectively. Finally,  $\mathbf{g}(\mathbf{x}_t, \mathbf{u}_t)$  is the non-linear observation function. In the case of the CSCIF, the state is decomposed into the split form  $\{\mathbf{x}_t, \mathbf{P}_{it} + \mathbf{P}_{dt}\}$ , where  $\mathbf{P}_{it}$  and  $\mathbf{P}_{dt}$  denote the independent and dependent covariances, respectively, of state  $\mathbf{x}_t$  at time  $t$ . In the point set registration problem, the independent part of the noise covariance  $\mathbf{P}_{it}$  denotes the noise that varies the position of the points in the data set; this is independent in the registration process. The dependent part of the noise covariance  $\mathbf{P}_{dt}$  denotes the correspondence error that depends on the last iterative result. After each iteration, the correspondence between the points of two point sets will be updated according to the present iterative transformation matrix. In previous studies, the estimated covariance in the time update is approximated by a Jacobian matrix (similar to the extended Kalman filter), which makes the result imprecise. This work presents the cubature-rule-based split covariance filtering method, which can approximate the third-order term. In addition, we transform the method into the recursive Bayesian filtering form. The algorithm is shown in Algorithm 1.

Note that in Algorithm 1, the time update is a linear process, while the measurement update is non-linear and approximated by the third-order cubature rule. Both the predicted covariance and the noise covariance in the measurement update are split as independent and dependent parts. This algorithm still leaves an open problem, that is, the choice of the value of  $\omega$ , which will be discussed in the next section.

## V. CSCIF-BASED POINT SET REGISTRATION

This section presents the point set registration algorithm based on the CSCIF derived above. Before adopting the CSCIF algorithm, two problems should be addressed here: the optimization of  $\omega$  and the choice of the covariance in both the process model and the observation model, saying  $\mathbf{Q}_{ik}$ ,  $\mathbf{Q}_{dk}$  and  $\mathbf{R}_{ik}$ ,  $\mathbf{R}_{dk}$ . The significance for optimization of  $\omega$  is due to the balance between dependent and independent error sources. Instead of setting it to a fixed value during registration, we tune it iteration by iteration by learning information online. To achieve this goal, Evolutionary Algorithm (EA) is used, which will be given in the following part. The reason for optimization of the covariances is to improve efficiency of the algorithm while guaranteeing convergence to the optimized value at the same time. This is achieved by using Continuous Simulated Annealing (CSA) algorithm, which will also be addressed in detail in the following part. After introducing these two heuristic algorithms for optimization of registration parameters, CSCIF based point set registration algorithm will be addressed at the end of this section.

**Algorithm 1** Cubature Split Covariance Intersection Filter**Time Update:**

- 1: Assume that at time  $k$ , the state and its covariance  $\{\hat{\mathbf{x}}_{t-1|t-1}, \mathbf{P}_{it|t-1} + \mathbf{P}_{dt|t-1}\}$  are known
- 2: Estimate the predictive state:  $\hat{\mathbf{x}}_{t|t-1} = \mathbf{F}_{t-1}\hat{\mathbf{x}}_{t-1|t-1}$
- 3: Estimate the predictive covariance as well as its independent and dependent parts:
 
$$\begin{aligned}\mathbf{P}_{t|t-1} &= \mathbf{F}_{t-1}\mathbf{P}_{t-1|t-1}\mathbf{F}_{t-1}^T + \mathbf{Q}_{t-1} \\ \mathbf{P}_{it|t-1} &= \mathbf{F}_{t-1}\mathbf{P}_{it-1|t-1}\mathbf{F}_{t-1}^T + \mathbf{Q}_{it-1} \\ \mathbf{P}_{dt|t-1} &= \mathbf{F}_{t-1}\mathbf{P}_{dt-1|t-1}\mathbf{F}_{t-1}^T + \mathbf{Q}_{dt-1} \\ \mathbf{P}_{1t|t-1} &= \mathbf{P}_{dt|t-1}/\omega_t + \mathbf{P}_{it|t-1}\end{aligned}$$

**Measurement Update:**

- 1: The measurement covariance:  $\mathbf{R}_t = \mathbf{R}_{dt}/(1 - \omega_t) + \mathbf{R}_{it}$
- 2: Factorize:  $\mathbf{P}_{1t|t-1} = \mathbf{S}_{t|t-1}\mathbf{S}_{t|t-1}^T$
- 3: Evaluate the cubature points ( $i = 1, 2, \dots, m$ ):
 
$$\mathbf{X}_{i,t|t-1} = \mathbf{S}_{t|t-1}\xi_i + \hat{\mathbf{x}}_{t|t-1}$$
- 4: Evaluate the propagated cubature points:
 
$$\mathbf{Y}_{i,t|t-1} = \mathbf{g}(\mathbf{X}_{i,t|t-1})$$
- 5: Estimate the predicted measurement:
 
$$\hat{\mathbf{y}}_{t|t-1} = \frac{1}{m} \sum_{i=1}^m \mathbf{Y}_{i,t|t-1}$$
- 6: Estimate the innovation covariance matrix:
 
$$\mathbf{P}_{yy,t|t-1} = \sum_{i=1}^m \mathbf{Y}_{i,t|t-1}\mathbf{Y}_{i,t|t-1}^T - \hat{\mathbf{y}}_{t|t-1}\hat{\mathbf{y}}_{t|t-1}^T + \mathbf{R}_t$$
- 7: Estimate the cross-covariance matrix:
 
$$\mathbf{P}_{xy,t|t-1} = \sum_{i=1}^m \mathbf{X}_{i,t|t-1}\mathbf{Y}_{i,t|t-1}^T - \hat{\mathbf{x}}_{t|t-1}\hat{\mathbf{y}}_{t|t-1}^T$$
- 8: Estimate the Kalman gain:  $\mathbf{K}_t = \mathbf{P}_{xy,t|t-1}\mathbf{P}_{yy,t|t-1}^{-1}$
- 9: Estimate the updated state:
 
$$\mathbf{x}_{t|t} = \hat{\mathbf{x}}_{t|t-1} + \mathbf{K}_t(\mathbf{y}_t - \hat{\mathbf{y}}_{t|t-1})$$
- 10: Estimate the corresponding covariance:
 
$$\begin{aligned}\mathbf{P}_{t|t} &= \mathbf{P}_{1t|t-1} - \mathbf{K}_t\mathbf{P}_{yy,t|t-1}\mathbf{K}_t^T \\ \mathbf{P}_{it|t} &= (\mathbf{I} - \mathbf{K}_t\mathbf{P}_{xy,t|t-1}\mathbf{P}_{1t|t-1})\mathbf{P}_{it|t-1} \\ &\times (\mathbf{I} - \mathbf{K}_t\mathbf{P}_{xy,t|t-1}^T\mathbf{P}_{1t|t-1})^T + \mathbf{K}_t\mathbf{R}_{it}\mathbf{K}_t^T \\ \mathbf{P}_{dt|t} &= \mathbf{P}_{t|t} - \mathbf{P}_{it|t}\end{aligned}$$

**A. Evolutionary-Algorithm-Based Optimization**

As mentioned above, we use EA to optimize the weight  $\omega$ . In this paper, we minimize  $\|\mathbf{P}_{k|k}\|$  with respect to  $\omega$ . The intuition behind it is that through tuning  $\omega$ , we want to minimize the covariance of the state, *i.e.*, minimize uncertainty of the point set registration result. Therefore, the problem is

$$\begin{aligned}\min_{\omega_k} f(\omega_k) &= \left\| \frac{1}{\omega_k} \mathbf{P}_{dk|t-1} - \mathbf{P}_{xy,k|k-1} \mathbf{P}_{yy,k|k-1}^{-1} \mathbf{P}_{xy,k|k-1}^T \right\|_0 \\ \text{subject to } 0 \leq \omega_t &\leq 1\end{aligned}\quad (20)$$

where

$$\begin{aligned}\mathbf{P}_{xy,t|t-1} &= \sum_{i=1}^m \mathbf{g}^T \left( \sqrt{\frac{1}{\omega_t} \mathbf{P}_{dt|t-1} + \mathbf{P}_{it|t-1} \xi_i + \hat{\mathbf{x}}_{t|t-1}} \right) \\ &\times \left( \sqrt{\frac{1}{\omega_t} \mathbf{P}_{dt|t-1} + \mathbf{P}_{it|t-1} \xi_i + \frac{m-1}{m} \hat{\mathbf{x}}_{t|t-1}} \right) \quad (21)\end{aligned}$$

$$\begin{aligned}\mathbf{P}_{yy,t|t-1} &= \sum_{i=1}^m \mathbf{g} \left( \sqrt{\frac{1}{\omega_t} \mathbf{P}_{dt|t-1} + \mathbf{P}_{it|t-1} \xi_i + \hat{\mathbf{x}}_{t|t-1}} \right)\end{aligned}$$

**Algorithm 2** EA-Based Optimization Algorithm

**Initialization:** Generate  $l$  candidates from a uniform distribution:  $\{\omega_1, \omega_2, \dots, \omega_l\} = \mathcal{U}(0, 1)$

**Do Until Converge:**

**Selection:**

- 1:  $\{\tilde{\omega}_1, \tilde{\omega}_2, \dots, \tilde{\omega}_l\} = \text{Sort}\{\omega_1, \omega_2, \dots, \omega_l\}$
- 2:  $\{\tilde{\Omega}_S = \{\tilde{\omega}_1, \tilde{\omega}_2, \dots, \tilde{\omega}_m\} = \{\tilde{\omega}_S^1, \tilde{\omega}_S^2, \dots, \tilde{\omega}_S^m\}$
- 3:  $\{\tilde{\Omega}_L = \{\tilde{\omega}_{m+1}, \tilde{\omega}_{m+2}, \dots, \tilde{\omega}_l\} = \{\tilde{\omega}_L^1, \tilde{\omega}_L^2, \dots, \tilde{\omega}_L^{l-m}\}$

**Crossover:**

- 1: Draw  $\alpha_i$  from uniform distribution  $\alpha_i \sim \mathcal{U}(0, \bar{\alpha})$
- 2:  $\tilde{\omega}_O^i = \alpha_i \tilde{\omega}_L^i + (1 - \alpha_i) \tilde{\omega}_S^k$

**Mutation:**

- 1:  $\tilde{\omega}_M^i = \begin{cases} \max\{\min\{2\tilde{\omega}_S^k - \tilde{\omega}_O^i, 1\}, 0\} & r_i \leq p_M \\ \tilde{\omega}_O^i & r_i > p_M \end{cases}$
- 2:  $\Omega = \{\tilde{\omega}_S^1, \tilde{\omega}_S^2, \dots, \tilde{\omega}_S^m, \tilde{\omega}_M^1, \tilde{\omega}_M^2, \dots, \tilde{\omega}_M^{l-m}\}$

**Terminate:** **for**  $k = T$  **to**  $k = T - 2$ :

$$\|f(\tilde{\omega}_{kS}^1) - f(\tilde{\omega}_{k-1S}^1)\| \leq \delta$$

$$\begin{aligned}&\times \mathbf{g}^T \left( \sqrt{\frac{1}{\omega_t} \mathbf{P}_{dt|t-1} + \mathbf{P}_{it|t-1} \xi_i + \hat{\mathbf{x}}_{t|t-1}} \right) + \frac{1}{1 - \omega_t} \mathbf{R}_{dt} \\ &- \frac{1}{m^2} \sum_{i=1}^m \mathbf{g} \left( \sqrt{\frac{1}{\omega_t} \mathbf{P}_{dt|t-1} + \mathbf{P}_{it|t-1} \xi_i + \hat{\mathbf{x}}_{t|t-1}} \right) \\ &\times \left( \sum_{i=1}^m \mathbf{g} \left( \sqrt{\frac{1}{\omega_t} \mathbf{P}_{dt|t-1} + \mathbf{P}_{it|t-1} \xi_i + \hat{\mathbf{x}}_{t|t-1}} \right) \right)^T \quad (22)\end{aligned}$$

This is a non-linear and non-convex optimization problem. A heuristic algorithm is adopted here to determine the value of  $\omega_k$ . In this paper, an evolutionary algorithm (EA) [24] is used to choose  $\omega$ . Inspired by the process of biological evolution, there are three steps involved in the EA: selection, crossover and mutation. The algorithm is depicted in Algorithm 2.

In Algorithm 2, the function  $\text{Sort}$  sorts the population in descending order according to the objective function  $f(\omega_k)$ . Then, the population is divided into two groups:  $\tilde{\Omega}_S$  and  $\tilde{\Omega}_L$ . In addition,  $m = \gamma N$ , where  $N$  is the cardinality of the subset whose objective function is smaller than the mean  $\sum_{i=1}^l f(\omega_i)$  and  $\gamma \in [0, 1]$  is a preset coefficient. The upper bound  $\bar{\alpha}$  is determined by  $\bar{\alpha} = 1 - \frac{N}{l}$ . When the L2 distance of the objective function on  $\omega_{S1}$  between two adjacent steps is no larger than the threshold  $\delta$  for three consecutive steps, the algorithm terminates.

**B. Continuous Simulated Annealing-Based Covariance Choice**

The covariance of the process noise  $\mathbf{Q}_{k-1}$  plays an important role in the recursive steps. The covariance makes the system dynamic and determines the domain that is explored. It slows the convergence when  $\mathbf{Q}_{k-1}$  is too large, and it may be unable to obtain the optimum solution. The best way to address this problem is to set  $\mathbf{Q}_{k-1}$  every step according to the filtering results. In this paper, CSA is utilized to set a proper noise covariance at each step. The algorithm is shown in Algorithm 3.

**Algorithm 3** Continuous Simulated Annealing**Input:**  $\mathbf{Q}_{k-1}$ ,  $\mathbf{y}_k$ ,  $\mathbf{y}_{k-1}$  and  $\mathbf{u}_k$ **Output:**  $\mathbf{Q}_k$ **Do**

- 1) Generate the candidate state:  $\tilde{\mathbf{Q}}_k = \mathbf{Q}_{k-1}$
- 2) Accept/reject the candidate state with the following rule:

Generate  $p$  from a uniform distribution  $\mathcal{U}(0, 1)$ 

$$\mathbf{Q}_k = \begin{cases} \tilde{\mathbf{Q}}_k & p < \mathcal{P}(\mathbf{y}_k, \mathbf{y}_{k-1}, \mathbf{u}_k, t_k) \\ \mathbf{Q}_{k-1} & \text{otherwise} \end{cases}$$

- 3) Cooling schedule determines  $t_{k+1}$

**Algorithm 4** CSCIF- Based Point Set Registration**Input:** point sets  $\mathbf{U}$  and  $\mathbf{Z}$ **Output:** transformation  $\theta = [\theta_x, \theta_y, \theta_z]$  and  $\mathbf{t} = [t_x, t_y, t_z]$ **Initialization:** state  $x_0$  with covariance  $\mathbf{P}_0$ , covariance of noise $\mathbf{Q}_0 = \mathbf{Q}_{i0} + \mathbf{Q}_{d0}$  and  $\mathbf{R}_0 = \mathbf{R}_{i0} + \mathbf{R}_{d0}$ **While** not converged **do**

- 1: CSCIF filtering in Algorithm 1
- 2: EA-based optimization of  $\omega$  in Algorithm 2
- 3: CSA-based covariance choice in Algorithm 3

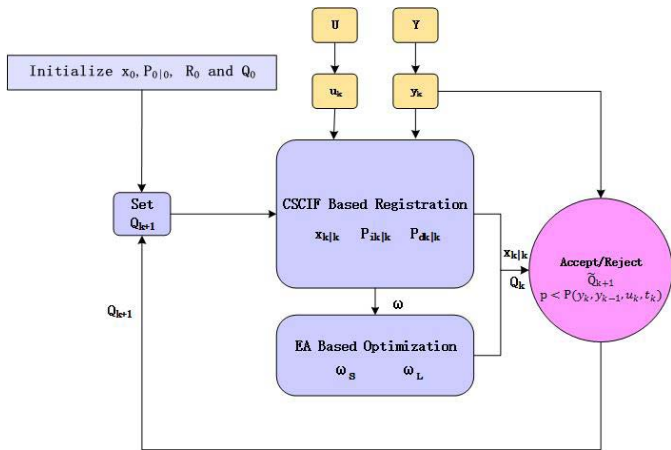
**End While**

Fig. 1. The flowchart of the registration algorithm.

where  $\mathcal{P}$  is an acceptance function defined as

$$\mathcal{P}(\mathbf{y}_k, \mathbf{y}_{k-1}, \mathbf{u}_k, t_k) = \min\{1, \frac{\bar{d}^{t_k}(\mathbf{y}_{k-1}, \mathbf{u}_k)}{\bar{d}^{t_k}(\mathbf{y}_k, \mathbf{u}_k)}\} \quad (23)$$

In addition, the function  $\bar{d}^{t_k}(\mathbf{y}_k, \mathbf{u}_k)$  measures the mean distance between the point set  $\mathbf{y}_k$  and the point set  $\mathbf{u}_k$  at the temperature  $t_k$ . Combining the previous three algorithms, the final CSCIF-based point set registration algorithm will be in the form shown in Algorithm 4. The chart of the complete algorithm is presented in Fig. 1.

## VI. EXPERIMENTAL RESULTS

First, we test the robustness of the proposed algorithm on a 2D data set with respect to noise, outliers and missing partial structures. Then, we proceed to test our algorithm

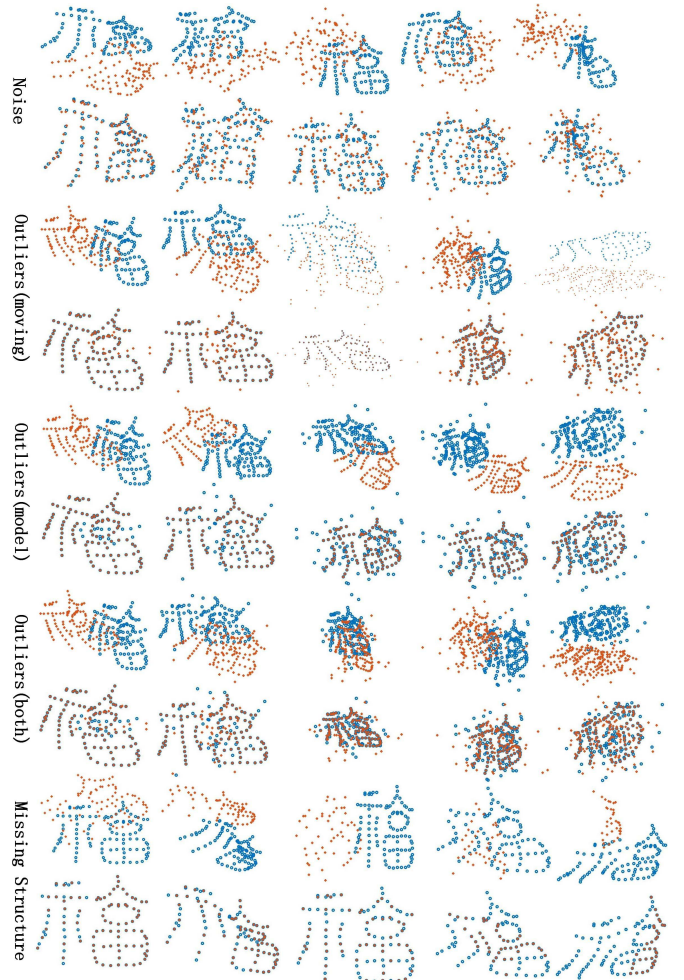


Fig. 2. Test of the CSCIF-based point set registration algorithm on the 2D dataset with respect to noise, outliers and missing partial structures.

on Stanford 3D point set data.<sup>1</sup> In the test, the robustness of the proposed algorithm to noise and outliers is emphasized. We also compare the robustness between the proposed algorithm and some state-of-the-art algorithms in terms of noise and outliers and various error sources simultaneously etc. Finally, the CSCIF-based point set registration algorithm is adopted in the map matching process of localization for autonomous vehicles.

## A. Test on 2D Data

The test is based on the widely used Chinese character dataset [25]. Three properties are tested in this 2D point set registration: robustness to noise, robustness to outliers and robustness to missing partial structures. The test result is shown in Fig. 2. In each test, the first row shows the original point sets, and the second row shows the two point sets after registration. For the noise test, white Gaussian noise is added to the Chinese character point set. The level of noise is measured by the ratio of the amplitude of the white Gaussian noise to the location of the points in the point set. Different

<sup>1</sup><http://graphics.stanford.edu/data/3Dscanrep/>

TABLE I  
AVERAGE REGISTRATION ERROR ON THE CHINESE CHARACTER DATASETS OF VARIOUS METHODS IN TERMS OF NOISE, OUTLIERS AND MISSING PARTIAL STRUCTURES OVER 100 TRIALS

Method	Noise				Outliers			100%	Missing Partial Structures				Misalignment Initialization			
	5%	15%	30%	40%	20%	40%	80%		10%	30%	50%	80%	10°	30°	50°	90°
ICP	0.03	0.13	0.39	0.81	0.03	0.08	0.18	0.27	0.17	0.46	0.82	1	0.04	0.25	0.76	1
GO-ICP	0.03	0.13	0.37	0.77	0.04	0.08	0.19	0.26	0.20	0.38	0.62	1	0.02	0.07	0.11	0.36
CPD	0.01	0.09	0.18	0.39	0.01	0.03	0.09	0.14	0.01	0.02	0.03	1	0.02	0.05	0.47	0.93
KC	0.02	0.10	0.21	0.41	0.04	0.05	0.12	0.18	0.02	0.05	0.30	1	0.02	0.06	0.38	0.90
PF	0.03	0.11	0.24	0.49	0.03	0.05	0.12	0.17	0.02	0.09	0.28	0.60	0.03	0.07	0.42	0.83
GMM-L2	0.01	0.10	0.21	0.40	0.03	0.05	0.09	0.11	0.01	0.03	0.04	0.58	0.02	0.06	0.37	0.90
CKF	0.01	0.06	0.16	0.25	0.01	0.03	0.08	0.13	0.02	0.15	0.33	0.62	0.01	0.01	0.04	0.09
CSCIF	0	0.07	0.10	0.17	0.02	0.03	0.03	0.05	0.02	0.05	0.04	0.30	0.01	0.01	0.03	0.06

levels of noise are illustrated in the figure from low to high (from left to right: 5%, 10%, 20%, 25% and 30%).

In the outliers test, three conditions are considered, *i.e.*, outliers added to the moving point set, outliers added to the model point set and outliers added to both point sets. The level of the outliers is measured by the ratio of the number of outliers points to the number of points in the original point set. The levels of the outliers increase from left to right (10%, 40%, 60%, 80% and 100%). In the partial structure test, some points in one point set are omitted. Various point-omitting strategies, such as omitting points in a specific area as well as omitting points either equally or randomly in the point set, are adopted here. The level of the partial structures is measured by the ratio of the number of omitted points to the number of points in the original point set. From the first to fifth column, the missing partial structure levels are 20%, 30%, 50%, 60% and 70%. From Fig. 2, it can be observed that the point set registration algorithm based on the CSCIF proposed in this paper is robust to noise, outliers and missing partial structures even under certain extreme conditions.

A comparison between the CSCIF-based point set registration and some state-of-the-art point set registration algorithms is presented in Table I with respect to noise, outliers, missing partial structures and misalignment initialization. The registration error is presented in each comparison for different levels of noise, outliers and missing partial structures. Here, the error is the ratio of the deviation of the transformation matrix between the noisy and non-noisy registration and the non-noisy transformation matrix. Seven registration algorithms are compared: the classical and widely used ICP [1], GO-ICP [14], CPD [2], Kernel Correlation (KC)-based point set registration [15], Particle Filtering (PF)-based point set registration [16], GMM-L2-based point set registration [3] and CKF based registration [12]. In the comparison of robustness to noise, the eight algorithms perform similarly when there is no noise or the noise level is low. As the noise level increases, the errors under certain methods (ICP and GO-ICP) increase significantly. From the table, it can be observed that the method proposed in this paper outperforms the first six methods with respect to noise substantially. Compared to the CKF based method, the proposed method is a little better, but the advantage is not that large. In the outliers test, it can be observed that the proposed CSCIF-based algorithm is hardly affected by outliers even when the outliers level is

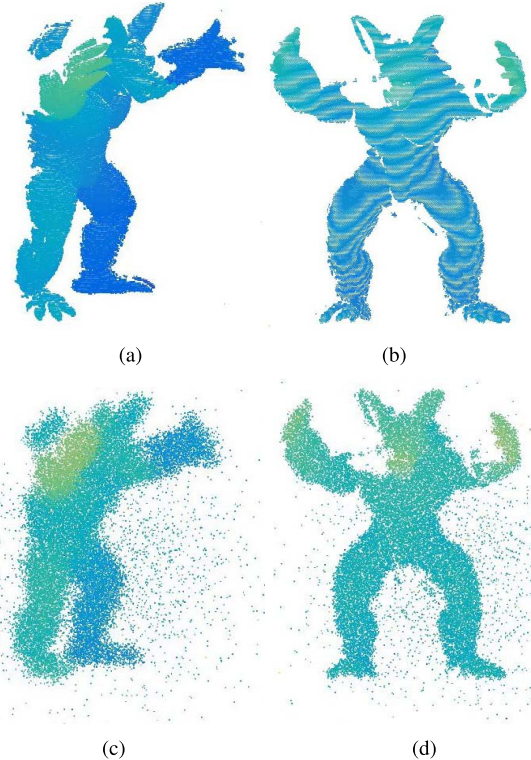


Fig. 3. An example of the point set before and after including noise. Differences of registration details are shown in red boxes. (a) ArmadollioStand120. (b) ArmadollioStand180. (c) ArmadollioStand120Noise. (d) ArmadollioStand180Noise.

one. The performance of the first six methods degrades when the outliers level increases. Error of CKF-based registration increases slowly as the level of outliers increases. In the missing partial structure test, we can see that the performance of the CSCIF-based algorithm hardly degrades when the missing partial structure level is lower than 0.5. On the other hand, the errors of the other methods increase significantly as the missing partial structure level increases. In particular, when the level is greater than 0.5, the errors from certain methods are as large as 1, which means that the registration under these methods fails completely. Error of CKF based registration increases quickly as the missing partial structure level increases, which is partly because of local shape descriptor used therein. There are two types of misalignment initialization:

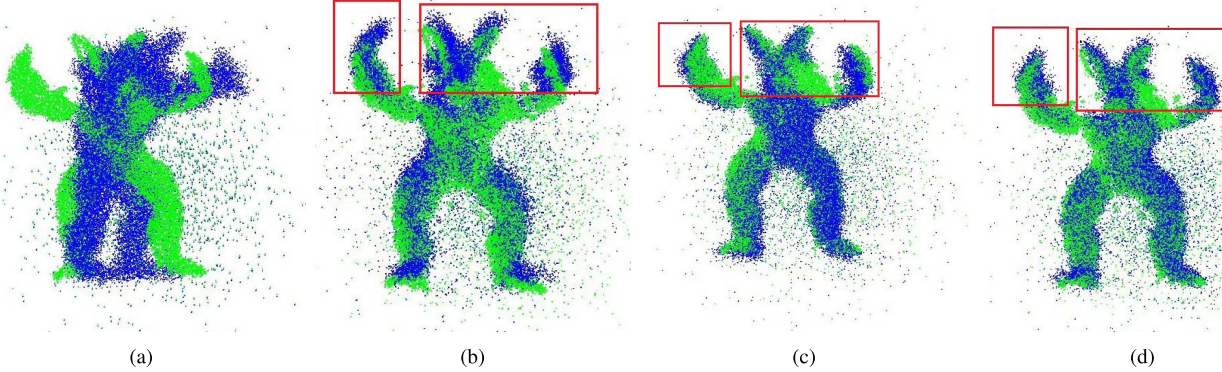


Fig. 4. The registration results of three different methods with noisy point sets. (a) GO-ICP. (b) CPD. (c) CKF. (d) CSCIF.

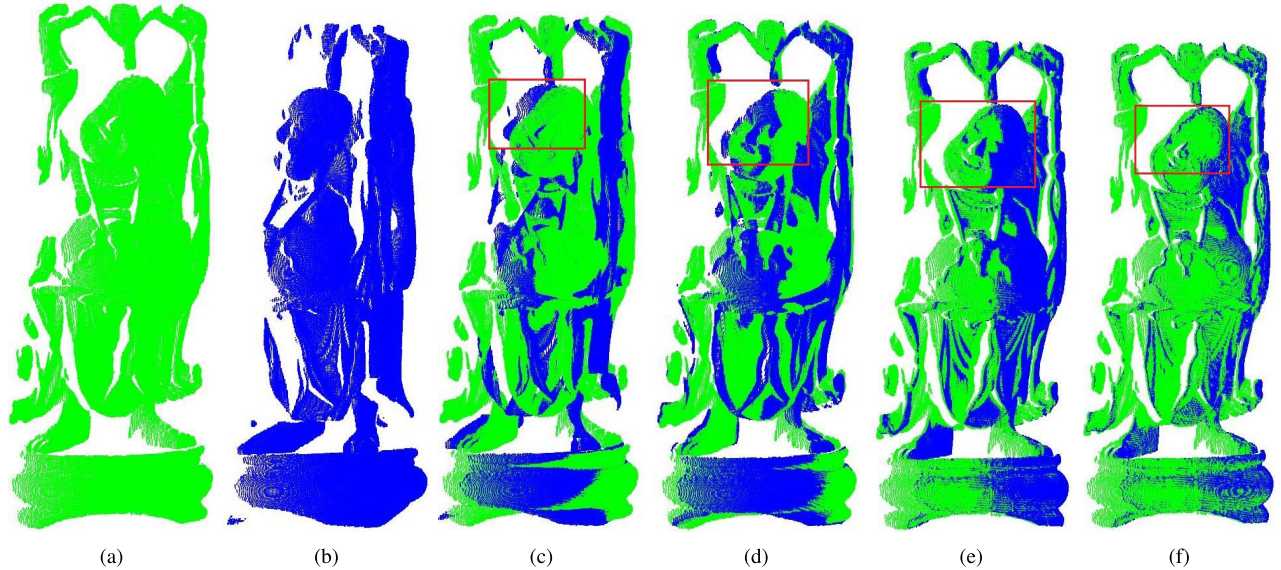


Fig. 5. Registration result in terms of misalignment initialization. Differences of registration details are shown in red boxes. (a) Original1. (b) Original2. (c) GO-ICP. (d) CPD. (e) CKF. (f) CSCIF.

translational and rotational initialization. An error in translational initialization is relatively easy to solve by moving the gravity center or the mean point center to the center of the other point set. Therefore, in this paper, the effects of errors in the rotational initialization are mainly investigated. From Table I, it can be seen that error of ICP increases quickly as the initial pose difference between the two point sets increases. The performance of GO-ICP improves obviously compared to ICP. CPD, KC, PF, and GMM-L2 perform well if the pose difference is smaller than  $30^\circ$ . If the difference is larger than  $50^\circ$ , errors of these four methods jump. When the difference reaches  $90^\circ$ , registration of these four methods almost fails. CKF- and CSCIF-based registration perform similarly, and the errors remain low even if the pose difference is  $90^\circ$ . From this test, the conclusion is CSCIF outperforms ICP, GO-ICP, CPD, KC, PF and GMM-L2 registration substantially in terms of noise, outliers, missing partial structures and misalignment initialization. Compared to CKF based registration, CSCIF performs a little better in terms of some tests, but the improvement is not substantial. Or, we can say CSCIF- and CKF-based point set registration perform similarly if there is only one single error source.

### B. Test on 3D Data

We use the Armadillo point set to test the robustness of the algorithm to noise and outliers. Here, we use the *ArmadilloStand120* and *ArmadilloStand180* point sets and add different levels of Gaussian noises to them. An example of a point set before and after including noise and outliers can be observed in Fig. 3. The registration results of four different methods are shown in Fig. 4. From the figure, it can be observed that GO-ICP fails to register the two point sets. CPD, CKF and CSCIF succeed in registering the two point sets. In addition, the registration details of the CSCIF outperform CPD and CKF a little bit.

We use the Happy Buddha point set to test the robustness of the algorithms to misalignment initialization. The results of *happyStandRight0* and *happyStandRight120* are shown in Fig. 5. In the figure, it can be observed that the CSCIF-based method registers the two point sets best. After registration, the two point sets coincide with each other. The CKF-based method performs the second best. The state-of-the-art methods, GO-ICP [14] and CPD [2], perform the third best. In particular, for GO-ICP, the distance between the registered point sets is obvious; see the face, body, etc. The test result on

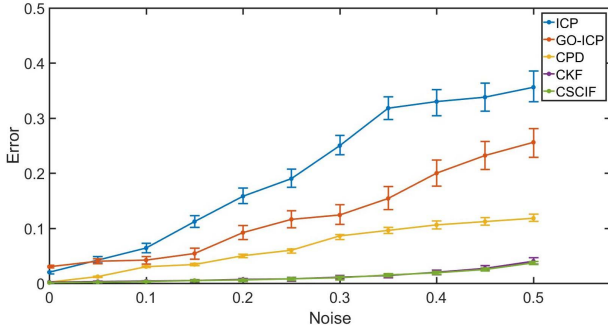


Fig. 6. Registration error under different levels of noises.

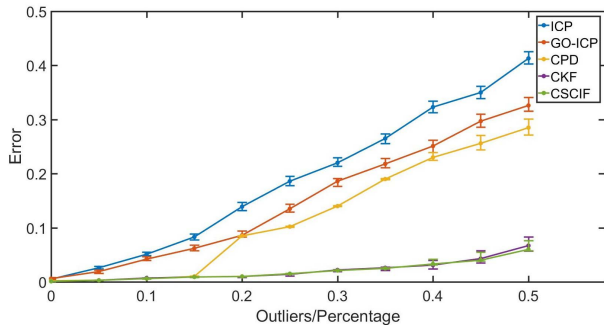


Fig. 7. Registration error under different levels of outliers.

the 3D point set is similar to that on the 2D point set; the errors of CSCIF- and CKF-based registration remain small even if the pose difference is larger than 90°, while the other methods fail to align the point sets in these cases.

We also test the registration performance of the original ICP, GO-ICP, CPD, CKF and CSCIF under different levels of noise, as illustrated in Fig. 6. This test is only about noise; therefore, outliers are not added. Here, the measurement of noise (*i.e.*, the x-axis) is the ratio between the mean of the Gaussian distribution of the noise and the mean of the point locations. In addition, the error is the deviation of the transformation matrix between the registration result and ground truth divided by the ground-truth transformation matrix. From the figure, it can be observed that the CSCIF-based method performs better than ICP, GO-ICP and CPD with respect to noise. CSCIF and CKF perform similarly in this test.

Next, the robustness of the algorithm under different levels of outliers is tested. Here, only outliers are added, and the results are shown in Fig. 7. The measurement of the outliers (*i.e.*, the x-axis) is the ratio between the number of outlier points and the number of points in the original point set. The error is defined in the same way as in the noise test. From the figure, it can be observed that the CSCIF-based method performs better than ICP, GO-ICP and CPD with respect to outliers. CSCIF and CKF also perform similarly in this case. Note that in both the noise and outliers tests, the noise and outliers are added to both the model point set and the moving point set.

From tests on the 2D and 3D point sets, it can be seen that CSCIF and CKF perform similarly in terms of noise, outliers and misalignment initialization. This is partly because

TABLE II  
TEST OF FUNCTION OF CSA AND EA

Method	CSCIF without CSA	CSCIF without EA	CSCIF
Time	510ms	113ms	76ms
Error	0.05	0.13	0.03

the filtering framework modeled point set registration and cubature rule-based nonlinearity approximation. These two methods outperform the other tested state-of-the-art or classic point set registration algorithms. However, the CKF-based method models all error sources as a uniform noise in the filtering framework, which may be questionable if there is more than one type of error source. We test the performance of CSCIF and CKF registration under two types of error sources, and the result is presented in Table III. The result is average registration error on both 2D and 3D point sets over 200 trials (100 on 2D point set and 100 on 3D point set). From the table, it can be seen that if more than one type of error source is added, the CKF-based method degenerates fast in some cases, while the CSCIF-based method does not degenerate substantially.

Finally, the functions of CSA and EA in the registration algorithm are tested. The aim of CSA is to improve the efficiency of the algorithm, so convergence speed is tested with and without CSA. We test the proposed method and the proposed method without CSA on 2D Chinese character datasets randomly over 100 trials, which means the point set may contain noise, outliers, misalignment initialization, both or all of them. The average convergence time is presented in Table II. After adopting CSA, the average convergence speed increases nearly seven times. The convergence time of CSCIF without EA is also presented. If adopting the algorithm without EA, the time consumed increases but does not decline as expected. This is because abandoning EA slows down the convergence speed to the true value or consumes more iterations to converge. The last row of Table II shows the registration errors of the proposed algorithm and the two variants of it. From the table, it can be seen that CSA does not affect the registration error much. But EA contributes to the precision of the proposed algorithm substantially.

### C. Real Platform Experiment

Some experiments on intelligent vehicles are presented and discussed in detail here. The application of the point set registration algorithm here is mainly metric map generation, map matching during localization and a combination of the two processes (*i.e.*, SLAM). First, a point cloud map is generated using SLAM, where the matching algorithm used in the front-end is the CSCIF based point set registration proposed in this paper. Then, we come to high-precision localization based on the transformation between the map generated above and the live local point cloud data. The computation of the transformation relies upon the CSCIF-based point set registration.

The sensor that we use is a Velodyne VLP-16 LIDAR mounted on the roof of a vehicle, as shown in Fig. 8.

TABLE III  
A COMPARISON BETWEEN CKF AND CSCIF BASED REGISTRATION BY AVERAGE REGISTRATION ERROR

Error Source	Noise				Outliers			Missing Partial Structures				Misalignment		Initialization				
	10%	20%	30%	40%	20%	40%	80%	100%	10%	30%	50%	80%	10°	30°	50°	90°		
CKF	Noise	10%	0.05	0.12	0.19	0.31	0.07	0.14	0.19	0.23	0.07	0.15	0.19	0.35	0.05	0.13	0.17	0.26
		20%	0.12	0.12	0.19	0.31	0.13	0.18	0.26	0.37	0.11	0.18	0.26	0.32	0.06	0.15	0.44	0.31
		30%	0.19	0.19	0.19	0.31	0.21	0.29	0.46	0.67	0.22	0.31	0.39	0.53	0.21	0.30	0.56	0.73
		40%	0.31	0.31	0.31	0.35	0.52	0.75	0.86	0.37	0.44	0.62	0.83	0.35	0.45	0.73	1	
	Outliers	20%	0.07	0.13	0.21	0.35	0.03	0.07	0.11	0.17	0.05	0.09	0.13	0.33	0.02	0.07	0.09	0.12
		40%	0.14	0.18	0.29	0.52	0.07	0.07	0.11	0.17	0.10	0.16	0.22	0.38	0.04	0.09	0.13	0.19
		80%	0.19	0.26	0.46	0.75	0.11	0.11	0.17	0.17	0.13	0.25	0.41	0.77	0.09	0.16	0.24	0.38
		100%	0.23	0.37	0.67	0.86	0.17	0.17	0.17	0.18	0.34	0.51	0.86	0.14	0.25	0.39	0.50	
	Partial	10%	0.07	0.11	0.22	0.37	0.05	0.10	0.13	0.18	0.03	0.16	0.29	0.57	0.03	0.05	0.06	0.09
		30%	0.17	0.24	0.31	0.44	0.16	0.18	0.25	0.34	0.16	0.16	0.29	0.57	0.17	0.18	0.18	0.22
		50%	0.29	0.36	0.39	0.62	0.31	0.32	0.41	0.51	0.29	0.29	0.57	0.29	0.30	0.32	0.36	
		80%	0.61	0.72	0.73	0.86	0.57	0.62	0.77	0.86	0.57	0.57	0.57	0.57	0.61	0.69	0.79	
CSCIF	Noise	10%	0.02	0.09	0.13	0.24	0.03	0.03	0.05	0.07	0.03	0.05	0.08	0.32	0.02	0.03	0.03	0.06
		20%	0.09	0.09	0.13	0.24	0.09	0.10	0.12	0.15	0.11	0.13	0.16	0.34	0.09	0.10	0.11	0.13
		30%	0.13	0.13	0.13	0.24	0.13	0.15	0.16	0.17	0.13	0.13	0.19	0.37	0.13	0.13	0.16	0.18
		40%	0.24	0.24	0.24	0.24	0.25	0.25	0.27	0.36	0.27	0.28	0.32	0.41	0.25	0.26	0.27	0.29
	Outliers	20%	0.03	0.09	0.13	0.25	0.03	0.03	0.04	0.07	0.03	0.05	0.05	0.30	0.03	0.04	0.06	0.07
		40%	0.03	0.10	0.15	0.25	0.03	0.03	0.04	0.07	0.03	0.06	0.06	0.31	0.04	0.04	0.06	0.07
		80%	0.05	0.12	0.16	0.27	0.04	0.04	0.07	0.07	0.05	0.06	0.08	0.33	0.05	0.06	0.07	0.08
		100%	0.07	0.15	0.17	0.36	0.07	0.07	0.07	0.07	0.07	0.09	0.36	0.07	0.07	0.09	0.10	
	Partial	10%	0.03	0.11	0.13	0.27	0.03	0.03	0.05	0.07	0.02	0.05	0.05	0.30	0.03	0.03	0.05	0.08
		30%	0.05	0.13	0.13	0.28	0.05	0.06	0.06	0.07	0.05	0.05	0.05	0.30	0.05	0.06	0.07	0.09
		50%	0.08	0.16	0.19	0.32	0.05	0.06	0.08	0.09	0.05	0.05	0.05	0.30	0.06	0.06	0.08	0.09
		80%	0.32	0.34	0.37	0.41	0.30	0.31	0.33	0.36	0.30	0.30	0.30	0.31	0.31	0.33	0.37	



Fig. 8. The platform used for the experiments in this paper. The red circle indicates the LiDAR used in this system, i.e., the Velodyne VLP-16.

The transformation between two consecutive frames of the scans is computed by the registration algorithm. In this way, the point cloud can be stitched together to generate the map. The initialization between the two consecutive frames (*e.g.*, registration initialization) relies upon the data from the IMU and the encoders. GPS provides the latitude and longitude of the point cloud. The map built in this way is shown in Fig. 9. In the map, details such as lamp posts, buildings, and trees retain their shapes, without warping or deformation, which verifies that the precision of the CSCIF-based point set registration algorithm is high.

Based on the map generated above, the vehicle can localize itself within this map. When it travels within the map, the transformation between the live data and the map can



Fig. 9. The map built using the CSCIF-based point set registration algorithm. (a) The scene. (b) The map built by the CSCIF.

be obtained by registering these two point clouds; in [12], it was verified that CKF outperforms ICP, NDT and CPD in the localization experiment. In this paper, we only focus on the performance of CKF- and CSCIF-based localization. The tests above indicate that the two algorithms perform similarly if there is only one type of error source. The advantage of CSCIF-based registration emerges if there is more than one type of error source. So, for the experiment, there are three factors to be considered:

1. We conducted this experiment in a congested urban environment full of vehicles and pedestrians. These could be viewed as outliers for point set registration.
2. The scanning frequency of the LiDAR is 10Hz, and the vehicle moves during the 100ms. Thus, the origin of the coordinate of points in the same frame changes as the vehicle moves. The LiDAR data are not corrected, which could be seen as noise for point set registration, and the level of the noise increases as the vehicle's velocity increases.
3. To improve efficiency, the map is stored as map pieces. Only the several nearby map pieces will be loaded for map matching. But the size of the map is much larger than the on-board data, which could be viewed as missing partial structures for point set registration.

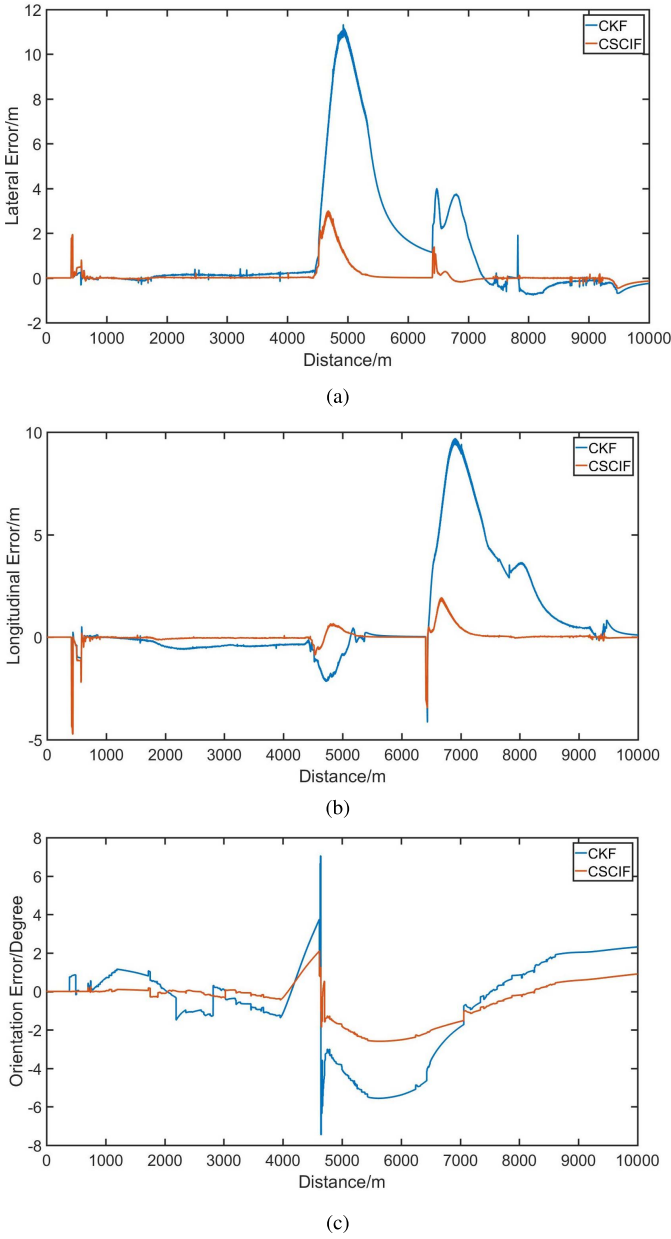


Fig. 10. Plots of localization in lateral, longitudinal and orientation. (a) Lateral error. (b) Longitudinal error. (c) Orientation error.

The experimental result is shown in Fig.10, where the ground truth is provided by the RTK-GPS. The test route is 10000m long in the congested urban environment. From the figure, it can be observed that the CSCIF-based registration algorithm is precise. It is also robust to outliers such as pedestrians and moving cars and noise brought by LiDAR data. Around 5000m, the lateral and orientation errors of CKF jump because the vehicle's velocity increases, which means the noise level increases a lot, while the CSCIF-based method is much more robust in this case. Around 7000m, the longitudinal error of CKF jumps because there is a canteen there in the campus and the number of pedestrians increases substantially. Again, the CSCIF-based method is much more robust in this case. When the registration cannot be completed in real time, the movement of the vehicle between two consecutive

TABLE IV  
MEAN ABSOLUTE ERROR AND MAXIMAL ERROR DURING LOCALIZATION

Method	MAE(x)	MAX(x)	MAE(y)	MAX(y)	MAE(o)	MAX(o)
CKF	1.29m	11.32m	1.31m	9.69m	0.78°	2.60°
CSCIF	0.16m	2.99m	0.15m	4.73m	1.83°	7.45°

CSCIF- and CKF-based results relies upon dead reckoning by the IMU. The statistics of the localization including Mean Absolute Error (MAE) and Maximal Error (MAX) are presented in Table IV.

## VII. CONCLUSIONS

In this paper, we presented a novel point set registration algorithm based on three main algorithms: CSCIF, EA and CSA. The dependent and independent parts of the covariance are considered separately; therefore, the registration is more precise and converges to the true value with high probability. The algorithm was shown to be robust to poor initialization, noise and outliers. Compared to heuristic methods (ICP, etc.), the local minimum problem can be averted by continuous simulated annealing for simultaneously exploring the probabilistic domain and converging to a specific domain quickly. Compared to probabilistic methods (CPD, etc.), robustness to noise, outliers, *etc.* has been improved substantially. Compared to other filtering-based methods (PF, UKF, EKF, etc.), this algorithm is consistent in the full domain of registration. Compared to our previous work, *i.e.*, CKF based point set registration [12], the proposed algorithm could deal with more than one error source much better. The limitation of this algorithm is that it currently cannot operate in real time for use by robots, and non-rigid registration has not been included in the present scheme; together with high-dimensional registration, this will be the direction of future work.

## REFERENCES

- [1] P. J. Besl and D. N. McKay, "A method for registration of 3-D shapes," *IEEE Trans. Pattern Anal. Mach. Intell.*, vol. 14, no. 2, pp. 239–256, Feb. 1992.
- [2] A. Myronenko and X. Song, "Point set registration: Coherent point drift," *IEEE Trans. Pattern Anal. Mach. Intell.*, vol. 32, no. 12, pp. 2262–2275, Dec. 2010.
- [3] B. Jian and B. C. Vemuri, "Robust point set registration using Gaussian mixture models," *IEEE Trans. Pattern Anal. Mach. Intell.*, vol. 33, no. 8, pp. 1633–1645, Aug. 2011.
- [4] M. H. Moghari and P. Abolmaesumi, "Point-based rigid-body registration using an unscented Kalman filter," *IEEE Trans. Med. Imag.*, vol. 26, no. 12, pp. 1708–1728, Dec. 2007.
- [5] P. Biber and W. Straßer, "The normal distributions transform: A new approach to laser scan matching," in *Proc. IEEE/RSJ Int. Conf. Intell. Robots Syst.*, vol. 3, Oct. 2003, pp. 2743–2748.
- [6] H. Durrant-Whyte and T. Bailey, "Simultaneous localization and mapping: Part I," *IEEE Robot. Autom. Mag.*, vol. 13, no. 2, pp. 99–110, Jun. 2006.
- [7] A. Rangarajan, H. Chui, and J. S. Duncan, "Rigid point feature registration using mutual information," *Med. Image Anal.*, vol. 3, no. 4, pp. 425–440, Dec. 1999.
- [8] A. Irschara, C. Zach, J.-M. Frahm, and H. Bischof, "From structure-from-motion point clouds to fast location recognition," in *Proc. IEEE Conf. Comput. Vis. Pattern Recognit.*, 2009, pp. 2599–2606.
- [9] A. M. Bazen and S. H. Gerez, "Fingerprint matching by thin-plate spline modelling of elastic deformations," *Pattern Recognit.*, vol. 36, no. 8, pp. 1859–1867, 2003.

- [10] C.-S. Chua, F. Han, and Y.-K. Ho, "3D human face recognition using point signature," in *Proc. IEEE Int. Conf. Autom. Face Gesture Recognit.*, Mar. 2000, pp. 233–238.
- [11] S. Belongie, J. Malik, and J. Puzicha, "Shape matching and object recognition using shape contexts," *IEEE Trans. Pattern Anal. Mach. Intell.*, vol. 24, no. 4, pp. 509–522, Apr. 2002.
- [12] L. Li, M. Yang, C. Wang, and B. Wang, "Rigid point set registration based on cubature Kalman filter and its application in intelligent vehicles," *IEEE Trans. Intell. Transp. Syst.*, vol. 14, no. 2, pp. 239–256, Feb. 1992.
- [13] S. Granger and X. Pennec, "Multi-scale EM-ICP: A fast and robust approach for surface registration," in *Proc. Eur. Conf. Comput. Vis.*, Copenhagen, Denmark, 2002, pp. 418–432.
- [14] J. Yang, H. Li, D. Campbell, and Y. Jia, "GO-ICP: A globally optimal solution to 3D icp point-set registration," *IEEE Trans. Pattern Anal. Mach. Intell.*, vol. 38, no. 11, pp. 2241–2254, Nov. 2015.
- [15] Y. Tsin and T. Kanade, "A correlation-based approach to robust point set registration," in *Proc. Eur. Conf. Comput. Vis.*, 2004, pp. 558–569.
- [16] R. Sandhu, S. Dambreville, and A. Tannenbaum, "Point set registration via particle filtering and stochastic dynamics," *IEEE Trans. Pattern Anal. Mach. Intell.*, vol. 32, no. 8, pp. 1459–1473, Aug. 2010.
- [17] S. J. Julier, "The scaled unscented transformation," in *Proc. IEEE Amer. Control Conf.*, vol. 6, May 2002, pp. 4555–4559.
- [18] R. P. Kanwal and K. C. Liu, "A Taylor expansion approach for solving integral equations," *Int. J. Math. Edu. Sci. Technol.*, vol. 20, no. 3, pp. 411–414, 1989.
- [19] A. H. Stroud, *Approximate Calculation of Multiple Integrals*. Englewood Cliffs, NJ, USA: Prentice-Hall, 1971.
- [20] I. Arasaratnam and S. Haykin, "Cubature Kalman filters," *IEEE Trans. Autom. Control*, vol. 54, no. 6, pp. 1254–1269, Jun. 2009.
- [21] S. J. Julier and J. K. Uhlmann, "A non-divergent estimation algorithm in the presence of unknown correlations," in *Proc. Amer. Control Conf.*, 1997, pp. 2369–2373.
- [22] S. J. Julier and J. K. Uhlmann, *General Decentralized Data Fusion With Covariance Intersection (CI)*. Boca Raton, FL, USA: CRC Press, 2001.
- [23] H. Li, F. Nashashibi, and M. Yang, "Split covariance intersection filter: Theory and its application to vehicle localization," *IEEE Trans. Intell. Transp. Syst.*, vol. 14, no. 4, pp. 1860–1871, Dec. 2013.
- [24] K. Deb, A. Pratap, S. Agarwal, and T. Meyarivan, "A fast and elitist multiobjective genetic algorithm: NSGA-II," *IEEE Trans. Evol. Comput.*, vol. 6, no. 2, pp. 182–197, Apr. 2002.
- [25] H. Chui and A. Rangarajan, "A new point matching algorithm for non-rigid registration," *Comput. Vis. Image Understand.*, vol. 89, nos. 2–3, pp. 114–141, Feb. 2003.



**Liang Li** (S'16) received the bachelor's degree in automation from the Harbin Institute of Technology, Harbin, China, in 2013. He is currently pursuing the Ph.D. degree with Shanghai Jiao Tong University, Shanghai, China.

His current research interests include high-precision localization for intelligent vehicles, computer vision, pattern recognition, outdoor high-precision localization for intelligent vehicles based on laser scanner, and computer vision methods.



**Ming Yang** received the master's and Ph.D. degrees from Tsinghua University, Beijing, China, in 1999 and 2003, respectively.

He is currently the Director of the Research Institute of Intelligent Vehicles Technology. He is also a Full Professor with the Department of Automation, Shanghai Jiao Tong University, Shanghai, China. He has been involved in the field of intelligent vehicles for over 20 years. He participated in several related research projects, such as the THMR-V project (first intelligent vehicle in China), European CyberCars and CyberMove projects, CyberC3 project, CyberCars-2 project, ITER transfer cask project, and AGV.



**Chunxiang Wang** received the Ph.D. degree in mechanical engineering from the Harbin Institute of Technology, Harbin, China, in 1999.

She is currently an Associate Professor with the Department of Automation, School of Electronic Information and Electrical Engineering, Shanghai Jiao Tong University, Shanghai, China. Her research interests include robotic technology and electro-mechanical integration.



**Bing Wang** received the Ph.D. degree in mechanical engineering from Shanghai Jiao Tong University, China, in 1997. He is currently a Senior Engineer with the Department of Automation, Shanghai Jiao Tong University. His research interests include embedded control, industrial automation, and automated guided vehicles.